Published in final edited form as:
Acta Biomater. 2012 November ; 8(11): 4053–4063. doi:10.1016/j.actbio.2012.07.024.

Hydroxyapatite Nanoparticle Reinforced Peptide Amphiphile Nanomatrix Enhances the Osteogenic Differentiation of Mesenchymal Stem Cells by Compositional Ratios

Jeremy B. Vines, **Dong-Jin Lim**, **Joel M. Anderson**, and **Ho-Wook Jun***
Department of Biomedical Engineering, University of Alabama at Birmingham, Birmingham, AL 35294, USA

Abstract

In the field of bone tissue engineering, there is a need for materials that mimic the native bone extracellular matrix (ECM). This need is met through the creation of biphasic composites intended to mimic both the organic and inorganic facets of the native bone ECM. However, few studies have created composites with organic ECM analogous components capable of directing cellular behaviors and many are not fabricated in the nanoscale. Furthermore, few attempts have been made at investigating how variations of organic and inorganic components affect the osteogenic differentiation of human mesenchymal stem cells (hMSCs). To address these issues, biphasic nanomatrix composites consisting of hydroxyapatite nanoparticles (HANPs) embedded within peptide amphiphile (PA) nanofibers tailored with the RGDS cellular adhesion motif (PA-RGDS) were created at various HANP to PA-RGDS ratios. Fabrication of these biphasic nanomatrix composites were confirmed via scanning electron microscope (SEM) and transmission electron microscope (TEM). The long-term cellularity and osteogenic differentiation of hMSCs in response to the different compositional ratios was then assessed by quantifying the timed expression of genes indicative of osteogenic differentiation, alkaline phosphatase activity, and DNA content over time. Decreased cellularity and the expression of genes over time correlated with increasing compositional ratios between HANP and PA-RGDS. The highest HANP to PA-RGDS ratio (66% HANP) exhibited the greatest improvement to the osteogenic differentiation of hMSCs. Overall, these results demonstrate that the compositional ratio of biphasic nanomatrix composites plays an important role in influencing the osteogenic differentiation of hMSCs. Based on the observations presented within this study, these biphasic nanomatrix composites show promise for future usage in bone tissue engineering applications.

1. Introduction

Research for the development of biomaterials for orthopedic applications has rapidly shifted to consider a tissue engineering approach that focuses on mimicking the native bone extracellular matrix (ECM) as opposed to biomaterials designed for the sole purpose of providing a load bearing replacement. This biomimetic approach involves the usage of materials capable of re-creating the native ECM microenvironment, which achieves its

*Corresponding author. Address: Department of Biomedical Engineering, University of Alabama at Birmingham, Shelby Building 806, 1825 University Boulevard, Birmingham, AL 35294, USA. Tel.: +1 205 996 6938; fax: +1 205 974 6938., hwjun@uab.edu (H.-W. Jun).

hierarchal construction through bottom-up self-assembly at the nanoscale level. The aim of this strategy is expedient regeneration and replacement of the scaffold with native bone tissue. By dispersing hydroxyapatite nanoparticles (HANPs) within a functionalized peptide amphiphile (PA) nanofiber matrix, we were able to successfully create a biphasic nanomatrix composite endowed with bioactivity derived from both the organic and inorganic facets of the native bone ECM. Supporting native osteogenic cells, the native bone ECM is a biphasic nanomatrix comprised of organic and inorganic components[1, 2] where organic collagen nanofibers are mineralized with reinforcing HANPs [3].

The organic ECM of bone, representing roughly ~20% of the native bone ECM by weight [2], is a network of proteins that directly regulates cellular behaviors through integrin mediated binding mechanisms [4]. PAs were designed to elicit the cell-ECM interactions normally provided by an organic ECM. PAs are bipolar molecules consisting of a hydrophilic peptide group attached to a hydrophobnic alkyl tail [5–7], self-assembling into cylindrical nanofibers approximately 8–10 nm in diameter under proper chemical conditions. The PA-driven material is versatile as the self-assembled nanofibers can form 3D hydrogels through the addition of divalent ions, or 2D multi-stacked layers through a solvent evaporation method [7–10]. These PAs have been modified through the incorporation of cellular adhesive ligand sequences isolated from common ECM proteins and peptide groups responsive to enzyme mediated degradation, providing microenvironments that capture the signaling properties of native ECM proteins and enzyme mediated degradation capability that does not lead to premature ECM erosion. Due to the customizable nature of the cellular adhesive ligand group, PAs have been utilized for a variety of tissue engineering fields such as cardiovascular, pancreatic, osteogenic, and drug delivery applications [8, 9, 11–13].

The native bone ECM serves to provide support for cells while also serving to regulate intercellular communication, influencing various cellular behaviors such as proliferation, migration, and differentiation [4, 14]. In an attempt to capture some of these properties, many studies have proposed the development of materials that mimic either the organic or inorganic aspects of the native bone ECM[15]. However, mimicking only one aspect of the biphasic ECM of bone may have limited success in eliciting sufficient osteogenic responses. To overcome this potential drawback, several groups have proposed the development of composites that mimic both the organic and inorganic facets of the native bone ECM. However, a majority of these studies involve the creation of composites utilizing synthetic polymers to serve as the organic ECM analogous component with HA serving as the inorganic ECM analogous component [16–20]. These synthetic polymers do not recreate the instructive microenvironment provided by native ECM proteins such as collagen without further modification. Additionally, a majority of these studies rely on fixed ratios between materials intended to serve as the organic and inorganic analogous ECM components[16, 21, 22], providing little insight into how compositional variations between the two ECM analogous components affect cellular response.

To address these issues, both the structural and biological properties of the native bone ECM were imitated by creating bone ECM analogous nanomatrix composites consisting of HANPs dispersed within PA nanofibers functionalized with the RGDS cellular adhesion motif (PA-RGDS). Furthermore, these biphasic nanomatrix composites were fabricated at various HANP to PA-RGDS ratios by weight to gain insightful knowledge about how compositional variations within the inorganic and organic ECM analogous components affects the osteogenic differentiation of human mesenchymal stem cells (hMSCs).

As described in our previous studies, it has been shown that these PAs, when functionalized with the RGDS cellular adhesion motif, are capable of inducing the osteogenic

differentiation of hMSCs both with and without the presence of osteogenic supplements [10, 23]. The RGD sequence has been shown to be one of the key cell binding domains present within the ECM, being found in multiple proteins such as fibronectin, vitronectin, fibrinogen, and osteopontin[24–26]. RGDS was chosen for this study as its incorporation into PAs has been shown to be the most conducive to the osteogenic differentiation of hMSCs relative to other cellular adhesive ligand sequences such as DGEA, which is derived from collagen, and KRSR which originates from various proteoglycans[10, 23].

While PA nanofiber matrices can promote and enhance the osteogenic differentiation of hMSCs, they only mimic the organic component of native bone ECM. To create a biphasic environment similar to that seen within the native bone ECM, HANPs were supplemented to serve as the inorganic ECM component. The inorganic phase of the native bone ECM is predominately made up of HA, representing roughly 70% of the ECM by weight[1, 2]. HA has seen increasing usage in bone graft therapies, both by itself and in combination with other bulk materials due to its improved bioactivity over traditional synthetic materials and previous studies have even proposed that HA has osteoinductive potential, although, this fact is contested [27–29]. However, while capable of providing bioactivity and potentially inducing osteogenic differentiation, HA, when utilized as a scaffold by itself, is slowly invaded by host tissues, demonstrating limited bioactive capacity when compared to native bone[30–32]. Therefore, to enhance bioactive capacity, HANPs were encapsulated within an organic ECM mimicking PA nanofiber matrix to create biphasic nanomatrix composites.

In order to assess the bioactive properties of these biphasic nanomatrix composites, hMSCs were introduced and long-term differentiation was measured. hMSCs are multi-potent cells capable of undergoing osteoblastic differentiation under various circumstances, usually with the aid of osteogenic supplement medium (OSM) (i.e. dexamethasone, β-glycerol phosphate). However, in a PA-guided microenvironment, hMSCs have been shown to undergo osteogenic differentiation in response to extracellular matrix-mimicking ligands and without the aid of OSM[10, 23].

In this study, the biphasic nanomatrix composite comprised of HANPs and PA-RGDS nanofibers was created to provide a bone analogous microenvironment. It was hypothesized that the osteogenic differentiation of hMSCs would be affected based on compositional ratios of HANP and PA-RGDS (Figure 1). These nanomatrix composites were fabricated and characterized using scanning electron microscope (SEM) and transmission electron microscope (TEM). Following this, the long-term cellularity and osteogenic differentiation of hMSCs was assessed *in vitro* utilizing quantitative real-time PCR (RT-PCR), Alkaline Phosphatase, Picogreen dsDNA, and Live/Dead assays. This study is thereby one of the first to assess the osteogenic differentiation of hMSCs in relation to variations in the ratio of organic and inorganic analogous ECM components capable of capturing both the nanoscale structure and bioactivity of the native bone ECM.

2. Methods and Materials

2.1 Peptide Amphiphile Synthesis

Peptide amphiphiles (PAs) were synthesized utilizing previously described methods [10, 23, 33]. Briefly, a peptide sequence consisting of a matrix metalloproteinase (MMP-2) enzyme mediated degradation sequence (GTAGLIGQ) and a cell adhesive ligand sequence (RGDS) was prepared using standard fluorenylmethyloxycarbonyl (Fmoc) chemistry in an Advanced Chemtech Apex 396 peptide synthesizer (Aapptec, Louisville, KY). Following this, a long alkyl chain was attached to the peptide sequence by reacting the *N*-termini with 2 equivalents of palmitic acid, 2 equivalents of *o*-benzotriazole-*N*,*N*,*N*′,*N*′ tetramethyluroniumhexafluorophosphate (HBTU), and 4 equivalents of

diisopropylethylamine (DiEA). The resin was cleaved through the addition of trifluoroacetic acid (TFA). Excess TFA was then removed through rotary evaporation, and the solution the precipitated in cold ether. Lastly, samples were lypophillized for 2–3 days, resulting in purified PA molecules. Proper fabrication of the PA was then confirmed via matrix-assisted laser desorption ionization time of flight (MALDI-TOF) mass spectrometry.

2.2 Preparation of Biphasic Nanomatrix Composites

PAs were first dissolved in filter sterilized DI water at 0.1% by weight, followed by pH neutralization through the addition of 1M NaOH. Autoclaved, crystalline hydroxyapatite nanoparticles (BABI-HAP-N100, Berkeley Advanced Biomaterials, Berkeley, CA) with an average diameter of 100 nm[34, 35] were then suspended within these solutions at various HANP to PA-RGDS ratios by weight (16%, 33%, 50%, and 66%) based on the amount of PA present per mL of solution (Table 1). Solutions were initially sonicated and vortexed to ensure the complete dispersion of HANPs within each PA solution. Under continuous stirring, 200 μL aliquots of each solution were placed into corresponding wells of a 48-well tissue culture plate (TCP; BD Biosciences, Sparks, MD). TCPs were placed into a non-humidifying incubator and gently shaken on a MTS 2/4 digital microtiter shaker (IKA WERKE GmbH & CO, Staufer, Germany), for 2 days to allow the formation of biphasic nanomatrix composites by solvent evaporation. The coated plates were then placed under a UV hood for 1 hour, followed by well rinsing using sterilized DI water 12 hours prior to cell seeding.

2.3 Transmission Electron Microscopy

HANPs and a 16% HANP nanomatrix composite were prepared on a carbon coated formvar copper grid (400 mesh) and dried for at least 4 hours in a chemical fume hood. The grids were then negatively stained with 2% phosphotungstic acid (PTA) buffered to pH 7 for 30 seconds. Excess solution was then wicked off the grid. Samples were imaged on a Tecnai T12 microscope (FEI, Hillsboro, OR) operated at 80 kV accelerating voltage.

2.4 Scanning Electron Microscopy

All biphasic nanomatrix composites were fabricated onto aluminum stubs utilizing solvent evaporation and characterized by a scanning electron microscope (SEM). Aluminum stubs were first sealed to create a well in which solution could be held and placed into a non-humidifying incubator. The amount of solution aliquoted to these stubs was scaled based on surface area relative to those formed on tissue culture plates. The composite coatings were then sputter coated with gold/palladium, and morphology was observed under a Quanta FEG 650 SEM (FEI, Hillsboro, OR) at an accelerating voltage of 20 kV.

2.5 Human Mesenchymal Stem Cell Culture

Human mesenchymal stem cells (hMSCs) were purchased from Lonza, Inc. (Lonza, Walkersville, MD), and only cells from passage numbers 4–6 were used. Cells were grown in Mesenchymal Stem Cell Basal Medium (Lonza, Walkersville, MD) supplemented with MSCBM SingleQuots (Lonza, Walkersville, MD). At confluency, cells were lifted from the culture surface and deactivated by adding a matching volume of Dulbecco's Modified Eagle's Medium (DMEM) supplemented with 10% Fetal Bovine Serum (HyClone, South Logan, UT), 1% Amphotericin B, 1% penicillin, 1% streptomycin (Mediatech, Manassas, VA), and 1% L-glutamine. Cells were then isolated through centrifugation at 1,000 RPM for 5 minutes and re-suspended at a concentration of 15,000 cells per 400 μL of osteogenic supplement medium (OSM) made by supplementing DMEM with 100 nM dexamethasone, 0.05 mg/mL L-abscorbic acid, and 10 mM β-glycerol phosphate (Sigma Aldrich, St. Louis, MO). 400μL aliquots of this solution were then transferred to the coated 48-well tissue

culture plates. Cell cultures were maintained under standard culture conditions (37°C, 95% relative humidity, 5% CO_2). Media was replaced with 400 μL of fresh media every 3–4 days.

2.6 Analysis of Cellularity

Cells were cultured and harvested through trypsinization at 1 hour for initial attachment and days 7, 14, and 28 for long-term cellularity. A Picogreen assay (Molecular Probes, Eugene, OR) was used to determine the DNA content according to manufacturer specifications. The DNA content was then measured on a fluorescent microplate reader (Synergy HT, BIO-TEK Instruments, Winooski, VT) filtered at 485/528 (EX/EM) and compared to a standard curve, correlating known DNA content. To determine the amount of cells per sample, hMSCs were determined to have 7.88×10^{-6}μg DNA per cell [10].

2.7 Alkaline Phosphatase Activity

Cells were cultured and collected at days 7, 14, and 28 through trypsinization and subjected to a freeze/thaw cycle. ALP activity was assessed using a fluorimetric SensoLyte FDP Alkaline Phosphatase Assay Kit (Anaspec, San Jose, CA). 50 μL aliquots of each sample were assayed for ALP content on a fluorescent microplate reader (Synergy HT, BIO-TEK Instruments, Winooski, VT) filtered at 485/528 (EX/EM) and compared to a standard correlating known ALP content to fluorescence levels. To normalize ALP expression by DNA content, a picogreen analysis was run to determine the specific ALP activity present within each sample.

2.8 Quantitative Real-Time Polymerase Chain Reaction (RT-PCR)

Cells were first collected and lysed with Trizol (Invitrogen, Carlsbad, CA) at days 7, 14, and 28. RNA was then isolated according to the Trizol protocol. Following isolation, the dried RNA pellet was re-suspended in nuclease-free water. To determine RNA concentration, a ND-1000 UV spectrophotometer (Nanodrop, Wilmington, DE) was used. 1 μg of RNA was then transferred to 0.2 mL eppendorf tubes for cDNA synthesis and reverse transcribed utilizing the iScript cDNA Synthesis Kit (Bio-Rad, Hercules, CA) per manufacturer's instructions. RT-PCR reactions were completed utilizing iQ SYBR Green Supermix (Bio-Rad, Hercules, CA) in an iQ5 Real-Time PCR machine (Bio-Rad, Hercules, CA). Reactions were cycled under the following parameters: 95°C for 3 min, 40 cycles at 95°C for 20 seconds, 55°C for 20 seconds, and 72°C for 20 seconds. The following primers (Runx2, ALP, OCN, and 18S) were used to evaluate gene expression (Table 2). To ensure primer specificity and check for genomic DNA contamination, melt-curve analysis was performed. The $2^{-\Delta\Delta CT}$ method was used to determine gene expression as previously described [23, 36]. Data was normalized by 18S and shown as a fold ratio relative to cells seeded on TCP cultured in OSM.

2.9 Cell Viability

Cells were cultured on biphasic nanomatrix composites for 7 days. At the respective time points, cells were rinsed with PBS and stained using a Live/Dead assay kit (Invitrogen, Carlsbad, CA) consisting of calcein AM and ethidium homodimer-1. The stained cells were imaged under fluorescence microscopy (Nikon TE2000-S; Nikon, Japan)

2.10 Statistical Analysis

The results presented are representative data sets with experiments performed three independent times with quadruplicate samples for each condition at each time point. All values were expressed as ± standard error of measurement. One-way analysis of variance (ANOVA) was performed using SPSS software (SPSS, Chicago, IL) to assess significant

differences between conditions at each time point. Tukey multiple comparison tests were further conducted to determine significant differences between pairs. For all tests, $p<0.05$ was considered significant.

3. Results

3.1 Scaffold Characterization

HANPs of around 100 nm diameter (Figure 2A) were suspended in a solution of PA-RGDS molecules following which, PA-RGDS molecules were induced into self-assembly. TEM imaging confirms the formation of cylindrical nanofibers 8–10 nm in diameter and several microns in length around small HANP aggregates 100–200 nm in diameter, forming nanomatrix composite coatings (Figure 2B). SEM imaging demonstrates a dose-wise increase in the HANP content between the 16% (Figure 2C), 33% (Figure 2D), 50% (Figure 2E) and 66% (Figure 2F) nanomatrix composite conditions. Due to the slightly hydrophobic nature of HA, HANPs tend to aggregate when dispersed in water. Variations in surface topography and slight increases in mean aggregate sizes were exhibited based on increases in the HANP to PA-RGDS ratios. SEM and TEM confirmed that biphasic nanomatrix composites could be successfully fabricated at various HANP to PA-RGDS ratios through the self-assembly of PA nanofibers around included HANPs.

3.2 Analysis of Cellularity

Initial seeding density of hMSCs was first determined by measuring adherent cells at the 1 hour time point (Figure 3). Overall, initial attachment was higher on the nanomatrix composite conditions incorporating HANPs with the greatest initial attachment occurring on the 16% HANP composite condition at a density of ~15,000 cells/cm^2. Of the nanomatrix composite conditions, initial attachment was the lowest on the 66% HANP nanomatrix composite condition. Following this, to determine changes to cell content over time, long-term cellularity was assessed over 28 days *in vitro*. By day 14, cellularity had changed in a fashion highlighting decreasing cell numbers based on increases in the HANP to PA-RGDS ratios. Cell number increased the most on TCP, with cells cultured on PA-RGDS demonstrating slightly less proliferation. The inclusion of HANPs into the PA nanofiber matrix further decreased cellularity based on increases in the HANP to PA-RGDS ratios, with the 50% and 66% HANP biphasic nanomatrix composites showing little increase in cellularity between days 7 and 28. Cells cultured on TCP and PA-RGDS exhibited the greatest cell numbers, approaching densities of ~85,000 cells/cm^2. In contrast, hMSCs cultured on the 66% HANP nanomatrix composite only approached a density of ~25,000 cells/cm^2, demonstrating little change to cell number over the course of the 28 day experiment. These results indicate that cellularity was inversely related to increases within the HANP to PA-RGDS ratios. Considering that proliferation is known to plateau at the onset of differentiation, it is possible that increases in the HANP to PA-RGDS ratio enhances osteogenic differentiation.

3.3 Cellular Viability

To ensure viability across all conditions, hMSCS were cultured for 7 days and stained with calcein AM and ethidium homodimer (Figure 4). No clear differences in terms of viability were found between the biphasic nanomatrix composites and PA-RGDS, implying that HANP incorporation did not have a detrimental effect on the viability of hMSCs.

3.4 Alkaline Phosphatase Activity

In order to assess mineralization, hMSCs were cultured on the nanomatrix composites over 28 days, following which, physical ALP activity was determined utilizing a quantitative biochemical assay (Figure 5). At day 7, there were no statistical differences amongst the

various conditions in terms of ALP activity. However, by day 14, ALP activity slightly increased based on increasing HANP to PA ratios. This trend continued into day 28 with ALP activity greatly increasing based on increases to the HANP to PA ratios with the 66% HANP composite condition exhibiting the greatest ALP activity.

3.5 Gene expression utilizing quantitative real time PCR

To confirm phenotypic commitment towards an osteogenic lineage, hMSCs were assessed for the up-regulation of genes specific to the temporal progression of osteogenic differentiation. To determine the onset of osteogenic commitment, Runx2 gene expression was assessed (Figure 6). At day 7, Runx2 was down-regulated on all surfaces relative to TCP with the exception of the 66% HANP composite condition, meaning that hMSCs had not begun their phenotypic commitment towards an osteogenic lineage with the exception of those cultured on the 66% HANP composite condition. By day 14, Runx2 had up-regulated in a step-wise fashion, signaling that early phenotypic commitment had begun to occur by day 14, with expression increasing based on increases to the HANP to PA-RGDS ratio. At day 28, Runx2 was slightly less expressed on all surfaces relative to TCP.

ALP gene expression appears to coincide with that of Runx2, as all but the 66% HANP condition did not demonstrate significant expression by the first week (Figure 7). However, by day 14, ALP expression was considerably higher than TCP, correlating with increases in the HANP to PA-RGDS ratio. Throughout the time-frame of the 28 day experiment, OCN expression is slowly up-regulated in a dose dependent fashion, with the greatest expression manifesting at the four weeks time point on the 66% HANP condition, indicating terminal differentiation relative to the other time points (Figure 8).

4. Discussion

In this study, we synthesized bone analogous nanomatrix composites that recreate the biphasic ECM of bone through the incorporation of organic ECM mimicking PA nanofibers tailored with the RGDS cellular adhesion motif and HANPs; the biphasic component was designed to satisfy the bone ECM structural characteristics in both nanoscale and bioactivity. Few studies have systematically investigated compositional variations in the ratio of inorganic to organic analogous ECM components on osteogenic differentiation, and a majority of studies assessed composite materials either at fixed ratios, or with an organic ECM analogous component that is not functionalized to provide signaling. Therefore, to assess changes to cellular behaviors, biphasic nanomatrix composites with increasing HANP to PA-RGDS ratios were studied and compared to PA-RGDS nanomatrix alone.

Biphasic nanomatrix composites were created utilizing a solvent evaporation method and characterized via SEM and TEM. TEM confirmed the successful self-assembly of PA nanofibers 8–10 nm in diameter around HANPs roughly 100 nm in diameter that appeared to form small aggregates. SEM demonstrated increasing HANP content between the 16%, 33%, 50%, and 66% nanomatrix composite conditions. By considering both the SEM and TEM images together, it appears that PA nanofibers are sandwiched in-between smaller HANP aggregates. These smaller aggregates are stacked on top of each other to form larger aggregates. As the HANP to PA-RGDS ratio was increased, there were slight increases to the size of the HANP/PA-RGDS aggregates, resulting in variations to surface topography. This is important since variations in surface topography have been shown to influence cellular behavior [37, 38]. HA is slightly hydrophobic by nature, thus, increasing the concentration of HANPs suspended within hydrophilic solutions of PA-RGDS resulted in larger HANP/PA-RGDS aggregates. The capability of self-assembly for the fabrication of composites provided by PAs may offer certain advantages over traditional fabrication methods. This is because fabricating biphasic nanomatrix composites in such a manner does

not require sintering and applied pressure to fixate HANPs through particle unification, thus potentially conserving grain size and improving nanoscale characteristics.

Functionalizing PAs takes advantage of an emerging strategy in which peptides are isolated from common ECM proteins to serve as cellular adhesive ligands, effectively mimicking the signaling capabilities of the native organic ECM [39–41]. PA-RGDS nanofibers were chosen to serve as the organic ECM analogous component since the included RGD sequence has shown potential in eliciting the osteogenic differentiation of hMSCs[10, 23]. RGDS is also common to multiple organic ECM proteins such as collagen and interacts with cells via the integrins α5-β1, α5-β3, and α2b-β3[42]. The combination of a PA-RGDS nanofiber matrix with HANPs in increasing HANP to PA-RGDS ratios was hypothesized to yield higher levels of osteogenic differentiation than a PA-RGDS nanofiber matrix alone. This is because numerous studies have demonstrated enhanced osteogenic differentiation when organic ECM proteins are combined with HA [43, 44]. Furthermore, it has been shown that HA can result in increased ALP activity, OPN secretion, and up-regulation of genes specific to osteoblastic activity [20, 45]. However, the exact mechanism(s) by which this may occur is unknown. Some proposed mechanisms by which HA may enhance osteogenic differentiation include variations in surface topography [37, 38], modification of surrounding media conditions with respect to increases in extracellular calcium and phosphate concentrations[45–49], and enhanced absorption of serum proteins [50–53].

Multiple groups have investigated biomimetic composites. However, few studies have assessed how the cellular behavior of osteoprogenitors changes in relation to the ratio between organic and inorganic analogous ECM components. Therefore, for this study, hMSCs were cultured on biphasic nanomatrix composites of varying HANP to PA-RGDS ratios and assessed for long-term differentiation. The first step in assessing the osteogenic differentiation of hMSCs was to investigate cellularity over time. By seeding hMSCs on these biphasic nanomatrix composites and assessing their cellularity over time, it was possible to determine cellular behaviors at the onset of osteogenic differentiation. Long-term phenomena such as proliferation and osteogenic gene expression appeared to correlate with changes in the HANP to PA-RGDS ratios. As noted earlier, overall cellularity was inversely related to the HANP to PA-RGDS ratio of each biphasic nanomatrix composite. To confirm the overall biocompatibility between the biphasic nanomatrix composites and hMSCs, viability imaging was performed. Live/Dead images demonstrated that there was no difference in terms of viability between PA-RGDS and the biphasic nanomatrix composites. These findings are supported by previous studies showing that HA does not negatively affect biocompatibility with osteogenic cell types [22, 54, 55].

Initial attachment demonstrated that the nanomatrix composites improved adherence when compared to the PA-RGDS control. However, amongst the various nanomatrix composite conditions, the greatest attachment occurred on the 16% HANP composite condition, demonstrating that differences in surface topography likely played a role. Differences in overall cell number were reflective of the initial time-frame upon which genes indicative of early osteogenic differentiation were expressed. The process of osteogenic differentiation occurs in three distinct stages. These stages take place in the following manner: cellular senescence, followed by matrix maturation, and finally, mineralization [56]. At the onset of differentiation, hMSCs slowly express genes indicative of an osteogenic cell type, such as alkaline phosphatase (ALP), osteocalcin (OCN), and runt related transcriptional factor 2 (Runx2). One of the earliest indications of osteoblastic differentiation is the expression of Runx2 [57], which has been demonstrated to be an essential mediator of cellular commitment towards an osteogenic lineage [58]. Runx2 had the greatest expression at the day 14 time point with expression increasing based on the HANP to PA-RGDS ratios. This expression pattern was inversely correlated with cell number, where increases to the HANP

to PA-RGDS ratio led to decreased cellularity at the same time point. As cellular senescence is an early event in the process of osteogenic differentiation[56, 59], the fact that it corresponded with the expression of genes indicative of early cellular commitment was expected. In this respect, multiple groups have demonstrated that Runx2 inhibits the proliferation of osteoprogenitor cells [60, 61]. Some studies investigating osteogenic differentiation in relation to HA concentration demonstrate similar patterns with respect to proliferation as well [45, 62]. In addition, PA-RGDS showed a statistically significant decrease in cell number relative to TCP over the course of the 28 day experiment, demonstrating that the cell to ligand interactions provided by the functionalized PA nanofibers serve to modify cellularity through osteogenic induction as well, confirming our results from previous studies [10, 23].

As differentiation proceeds, ALP activity increases, cleaving organic phosphates to produce free, inorganic phosphates in order to prepare the organic ECM for mineralization [46, 63], and has become an important indicator of osteogenic differentiation. ALP is slowly up-regulated over time with significant expression occurring during mid-term differentiation [57, 64]. OCN also plays an important role in the mineralization process, serving as a calcium binding protein. OCN up-regulation typically indicates a shift from middle to late term osteogenic differentiation [57, 64]. Further gene expression analysis of ALP and OCN displayed similar patterns in which the timed expression of middle and late term markers of osteogenic differentiation were enhanced by increasing the HANP to PA-RGDS ratios. Physical measurement of ALP activity confirms these results, demonstrating enhanced activity with regard to increasing HANP to PA-RGDS ratios. Based on these results, it is implicated that the biphasic nanomatrix composites regulate cellularity and osteogenic differentiation based on the ratio of the inorganic to organic analogous ECM components.

So far, whether osteogenic differentiation is enhanced or delayed by the incorporation of organic ECM proteins with HA is unclear and inconsistent. Some groups have previously reported that the combination of various organic ECM proteins such as collagen with HA can enhance osteogenic differentiation relative to HA alone [43, 44]. However, in other studies, results claim that the incorporation of organic ECM proteins enhances proliferation over time [65, 66]; this is a behavior that would seem to indicate delayed differentiation since cellularity plateaus at the onset of osteogenic differentiation. However, our findings demonstrate a combinatory effect between PA-RGDS and HANPs, giving weight to the claim that these biphasic nanomatrix composites enhance osteogenic differentiation when compared to an organic ECM analogous nanomatrix alone.

Unfortunately, as mentioned earlier, the mechanism(s) by which this combinatory effect occurs has not been elucidated. Due to the fact that various factors such as surface topography, extracellular calcium concentration, and the enhanced serum absorption caused by HA inclusion have been demonstrated to affect osteogenic differentiation, it is unclear as to how increasing the HANP to PA-RGDS ratios elicited enhanced osteogenic differentiation, highlighting a limiting factor to this study. In the future, the conclusions of this study can be enhanced by assessing variations in factors such as surface topography in relation to the extracellular matrix component ratios.

5. Conclusion

For this study, we developed a biphasic, bone analogous nanomatrix composite capable of recapturing both the structural properties and bioactivity of the native bone ECM. This was achieved by encapsulating HANPs within a self-assembled PA-RGDS nanomatrix. In order to determine how compositional variations influence the osteogenic differentiation of hMSCs, the biphasic nanomatrix composites were fabricated at various HANP to PA-RGDS

ratios. SEM and TEM imaging confirmed the successful formation of biphasic nanomatrix composites with increasing HANP content. Long-term observation of cellular response showed that the osteogenic differentiation of hMSCs seeded on the biphasic nanomatrix composites was regulated based on the ratio of inorganic to organic analogous ECM components, with the greatest enhancement occurring on the composites with the highest HANP to PA-RGDS ratios. These conclusions were reached based on the fact that plateaued cell number and the timed expression of genes indicative of osteogenic differentiation corresponded to increases within the HANP to PA-RGDS ratios, building upon previous studies demonstrating a combinatory effect between HANPs and PA-RGDS. In this study, the importance for a biphasic composite that mimics the native bone extracellular matrix (ECM) was addressed. This study was one of the first to assess the osteogenic differentiation of hMSCs in relation to variations in the ratio of organic and inorganic analogous ECM components capable of capturing both the nanoscale structure and bioactivity of the native bone ECM. Overall, the biphasic nanomatrix composites enhanced the differentiation of hMSCs, demonstrating their potential for usage in bone tissue engineering applications.

Acknowledgments

I wish to acknowledge the Mass Spectrometry/Proteomics Shared facility at UAB for analyzing all the PA samples. Thanks to Dr. Robin Foley for usage of the SEM facilities. Special thanks are also extended to Dr. Ralph Sanderson for use of his RT-PCR lab facilities and further to Dr. Vishnu Ramani for his help with all of the RT-PCR experiments and for providing the helpful advice necessary for the optimization and improvement of cell culture conditions. This work was supported by the NSF Career Award (CBET-0952974), Wallace H. Coulter Foundation, and UAB BERM center pilot grant awarded to H.-W.J., along with funding from NIH T32 predoctoral training grant (NIBIB #EB004312-01) and Ruth L. Kirschstein National Research Service Award Individual Fellowship (1F31DE021286-01) for J.M.A.

References

1. Clarke B. Normal bone anatomy and physiology. Clinical journal of the American Society of Nephrology: CJASN. 2008; 3 (Suppl 3):S131–9. [PubMed: 18988698]
2. Ashman, RF.; Buckwalter, JA.; Devane, P.; Dobbs, MB.; Ferguson, PJ.; Flatow, EL., et al. Turek's Orthopaedics: Principles and Their Application. 6. Iowa City: Lippincott Williams and Wilkins; 2005.
3. Bonzani IC, George JH, Stevens MM. Novel materials for bone and cartilage regeneration. Current opinion in chemical biology. 2006; 10:568–75. [PubMed: 17011226]
4. Couchman JR, Austria MR, Woods A. Fibronectin-cell interactions. The Journal of investigative dermatology. 1990; 94:7S–14S. [PubMed: 2191056]
5. Hartgerink JD, Beniash E, Stupp SI. Self-assembly and mineralization of peptide-amphiphile nanofibers. Science. 2001; 294:1684–8. [PubMed: 11721046]
6. Beniash E, Hartgerink JD, Storrie H, Stendahl JC, Stupp SI. Self-assembling peptide amphiphile nanofiber matrices for cell entrapment. Acta biomaterialia. 2005; 1:387–97. [PubMed: 16701820]
7. Jun HW, Yuwono V, Paramonov SE, Hartgerink JD. Enzyme-mediated degradation of peptide-amphiphile nanofiber networks. Adv Mater. 2005; 17:2612.
8. Andukuri A, Minor WP, Kushwaha M, Anderson JM, Jun HW. Effect of endothelium mimicking self-assembled nanomatrices on cell adhesion and spreading of human endothelial cells and smooth muscle cells. Nanomedicine: nanotechnology, biology, and medicine. 2010; 6:289–97.
9. Kushwaha M, Anderson J, Minor W, Andukuri A, Bosworth C, Lancaster J, et al. Native Endothelium Mimicking Self-assembled Nanomatrix for Cardiovascular Devices. Biomaterials. 2010; 31:1502–8. [PubMed: 19913295]
10. Anderson JM, Kushwaha M, Tambralli A, Bellis SL, Camata RP, Jun HW. Osteogenic differentiation of human mesenchymal stem cells directed by extracellular matrix-mimicking ligands in a biomimetic self-assembled peptide amphiphile nanomatrix. Biomacromolecules. 2009; 10:2935–44. [PubMed: 19746964]

11. Kim JK, Anderson J, Jun HW, Repka MA, Jo S. Self-assembling peptide amphiphile-based nanofiber gel for bioresponsive cisplatin delivery. Molecular pharmaceutics. 2009; 6:978–85. [PubMed: 19281184]
12. Lim DJ, Antipenko SV, Anderson JM, Jaimes KF, Viera L, Stephen BR, et al. Enhanced rat islet function and survival in vitro using a biomimetic self-assembled nanomatrix gel. Tissue engineering Part A. 2011; 17:399–406. [PubMed: 20807014]
13. Lim DJ, Antipenko SV, Andukuri A, Corbett JA, Jun HW. Biological sensitivity to self-assembled nanomatrix platforms depends on the phenotype of MIN6 beta-cells. Micro Nano Lett. 2011; 6:619–23.
14. Keselowsky BG, Collard DM, Garcia AJ. Integrin binding specificity regulates biomaterial surface chemistry effects on cell differentiation. Proceedings of the National Academy of Sciences of the United States of America. 2005; 102:5953–7. [PubMed: 15827122]
15. Supova M. Problem of hydroxyapatite dispersion in polymer matrices: a review. Journal of materials science. 2009; 20:1201–13. [PubMed: 19225871]
16. Huang J, Di Silvio L, Wang M, Tanner KE, Bonfield W. In vitro mechanical and biological assessment of hydroxyapatite-reinforced polyethylene composite. Journal of materials science. 1997; 8:775–9. [PubMed: 15348789]
17. Patlolla A, Collins G, Arinzeh TL. Solvent-dependent properties of electrospun fibrous composites for bone tissue regeneration. Acta biomaterialia. 2010; 6:90–101. [PubMed: 19631769]
18. Thomas V, Jagani S, Johnson K, Jose MV, Dean DR, Vohra YK, et al. Electrospun bioactive nanocomposite scaffolds of polycaprolactone and nanohydroxyapatite for bone tissue engineering. Journal of nanoscience and nanotechnology. 2006; 6:487–93. [PubMed: 16573049]
19. Venugopal J, Low S, Choon AT, Kumar AB, Ramakrishna S. Electrospun-modified nanofibrous scaffolds for the mineralization of osteoblast cells. Journal of biomedical materials research Part A. 2008; 85:408–17. [PubMed: 17701970]
20. He J, Genetos DC, Leach JK. Osteogenesis and trophic factor secretion are influenced by the composition of hydroxyapatite/poly(lactide-co-glycolide) composite scaffolds. Tissue engineering Part A. 2010; 16:127–37. [PubMed: 19642853]
21. Kim SS, Ahn KM, Park MS, Lee JH, Choi CY, Kim BS. A poly(lactide-co-glycolide)/ hydroxyapatite composite scaffold with enhanced osteoconductivity. Journal of biomedical materials research Part A. 2007; 80:206–15. [PubMed: 17072849]
22. Lao L, Wang Y, Zhu Y, Zhang Y, Gao C. Poly(lactide-co-glycolide)/hydroxyapatite nanofibrous scaffolds fabricated by electrospinning for bone tissue engineering. Journal of materials science. 2011; 22:1873–84. [PubMed: 21681656]
23. Anderson JM, Vines JB, Patterson JL, Chen H, Javed A, Jun HW. Osteogenic differentiation of human mesenchymal stem cells synergistically enhanced by biomimetic peptide amphiphiles combined with conditioned medium. Acta biomaterialia. 2011; 7:675–82. [PubMed: 20728586]
24. Bongio M, van den Beucken JJ, Nejadnik MR, Leeuwenburgh SC, Kinard LA, Kasper FK, et al. Biomimetic modification of synthetic hydrogels by incorporation of adhesive peptides and calcium phosphate nanoparticles: in vitro evaluation of cell behavior. European cells & materials. 2011; 22:359–76. [PubMed: 22179935]
25. Barczyk M, Carracedo S, Gullberg D. Integrins. Cell and tissue research. 2010; 339:269–80. [PubMed: 19693543]
26. Pierschbacher MD, Ruoslahti E. Variants of the cell recognition site of fibronectin that retain attachment-promoting activity. Proceedings of the National Academy of Sciences of the United States of America. 1984; 81:5985–8. [PubMed: 6237366]
27. Muller P, Bulnheim U, Diener A, Luthen F, Teller M, Klinkenberg ED, et al. Calcium phosphate surfaces promote osteogenic differentiation of mesenchymal stem cells. Journal of cellular and molecular medicine. 2008; 12:281–91. [PubMed: 18366455]
28. Kang SW, Lee JS, Park MS, Park JH, Kim BS. Enhancement of in vivo bone regeneration efficacy of human mesenchymal stem cells. Journal of microbiology and biotechnology. 2008; 18:975–82. [PubMed: 18633301]

29. Xie J, Baumann MJ, McCabe LR. Osteoblasts respond to hydroxyapatite surfaces with immediate changes in gene expression. Journal of biomedical materials research Part A. 2004; 71:108–17. [PubMed: 15368260]
30. Matsumine A, Myoui A, Kusuzaki K, Araki N, Seto M, Yoshikawa H, et al. Calcium hydroxyapatite ceramic implants in bone tumour surgery. A long-term follow-up study. The Journal of bone and joint surgery British volume. 2004; 86:719–25. [PubMed: 15274270]
31. White E, Shors EC. Biomaterial aspects of Interpore-200 porous hydroxyapatite. Dental clinics of North America. 1986; 30:49–67. [PubMed: 3514293]
32. Vuola J, Taurio R, Goransson H, Asko-Seljavaara S. Compressive strength of calcium carbonate and hydroxyapatite implants after bone-marrow-induced osteogenesis. Biomaterials. 1998; 19:223–7. [PubMed: 9678871]
33. Anderson JM, Andukuri A, Lim DJ, Jun HW. Modulating the gelation properties of self-assembling peptide amphiphiles. ACS nano. 2009; 3:3447–54. [PubMed: 19791757]
34. Crowley J, Chalivendra VB. Mechanical characterization of ultra-high molecular weight polyethylene-hydroxyapatite nanocomposites. Bio-medical materials and engineering. 2008; 18:149–60. [PubMed: 18725695]
35. Kim K, Dean D, Lu A, Mikos AG, Fisher JP. Early osteogenic signal expression of rat bone marrow stromal cells is influenced by both hydroxyapatite nanoparticle content and initial cell seeding density in biodegradable nanocomposite scaffolds. Acta biomaterialia. 2011; 7:1249–64. [PubMed: 21074640]
36. Schmittgen TD, Livak KJ. Analyzing real-time PCR data by the comparative C(T) method. Nature protocols. 2008; 3:1101–8.
37. Lincks J, Boyan BD, Blanchard CR, Lohmann CH, Liu Y, Cochran DL, et al. Response of MG63 osteoblast-like cells to titanium and titanium alloy is dependent on surface roughness and composition. Biomaterials. 1998; 19:2219–32. [PubMed: 9884063]
38. Brett PM, Harle J, Salih V, Mihoc R, Olsen I, Jones FH, et al. Roughness response genes in osteoblasts. Bone. 2004; 35:124–33. [PubMed: 15207748]
39. Carson AE, Barker TH. Emerging concepts in engineering extracellular matrix variants for directing cell phenotype. Regenerative medicine. 2009; 4:593–600. [PubMed: 19580407]
40. Barker TH. The role of ECM proteins and protein fragments in guiding cell behavior in regenerative medicine. Biomaterials. 2011; 32:4211–4. [PubMed: 21515169]
41. Lee JY, Choo JE, Park HJ, Park JB, Lee SC, Jo I, et al. Injectable gel with synthetic collagen-binding peptide for enhanced osteogenesis in vitro and in vivo. Biochemical and biophysical research communications. 2007; 357:68–74. [PubMed: 17418806]
42. Hersel U, Dahmen C, Kessler H. RGD modified polymers: biomaterials for stimulated cell adhesion and beyond. Biomaterials. 2003; 24:4385–415. [PubMed: 12922151]
43. Sogo Y, Ito A, Matsuno T, Oyane A, Tamazawa G, Satoh T, et al. Fibronectin-calcium phosphate composite layer on hydroxyapatite to enhance adhesion, cell spread and osteogenic differentiation of human mesenchymal stem cells in vitro. Biomedical materials. 2007; 2:116–23. [PubMed: 18458444]
44. Hennessy KM, Pollot BE, Clem WC, Phipps MC, Sawyer AA, Culpepper BK, et al. The effect of collagen I mimetic peptides on mesenchymal stem cell adhesion and differentiation, and on bone formation at hydroxyapatite surfaces. Biomaterials. 2009; 30:1898–909. [PubMed: 19157536]
45. Liu Y, Wang G, Cai Y, Ji H, Zhou G, Zhao X, et al. In vitro effects of nanophase hydroxyapatite particles on proliferation and osteogenic differentiation of bone marrow-derived mesenchymal stem cells. Journal of biomedical materials research Part A. 2009; 90:1083–91. [PubMed: 18671263]
46. Beck GR Jr. Inorganic phosphate as a signaling molecule in osteoblast differentiation. J Cell Biochem. 2003; 90:234–43. [PubMed: 14505340]
47. Khoshniat S, Bourgine A, Julien M, Petit M, Pilet P, Rouillon T, et al. Phosphate-dependent stimulation of MGP and OPN expression in osteoblasts via the ERK1/2 pathway is modulated by calcium. Bone. 2011; 48:894–902. [PubMed: 21147284]
48. Liu YK, Lu QZ, Pei R, Ji HJ, Zhou GS, Zhao XL, et al. The effect of extracellular calcium and inorganic phosphate on the growth and osteogenic differentiation of mesenchymal stem cells in

vitro: implication for bone tissue engineering. Biomedical materials. 2009; 4:025004. [PubMed: 19208939]

49. Maeno S, Niki Y, Matsumoto H, Morioka H, Yatabe T, Funayama A, et al. The effect of calcium ion concentration on osteoblast viability, proliferation and differentiation in monolayer and 3D culture. Biomaterials. 2005; 26:4847–55. [PubMed: 15763264]
50. El-Ghannam A, Ducheyne P, Shapiro IM. Effect of serum proteins on osteoblast adhesion to surface-modified bioactive glass and hydroxyapatite. J Orthop Res. 1999; 17:340–5. [PubMed: 10376721]
51. Kilpadi KL, Chang PL, Bellis SL. Hydroxylapatite binds more serum proteins, purified integrins, and osteoblast precursor cells than titanium or steel. J Biomed Mater Res. 2001; 57:258–67. [PubMed: 11484189]
52. Rosengren A, Pavlovic E, Oscarsson S, Krajewski A, Ravaglioli A, Piancastelli A. Plasma protein adsorption pattern on characterized ceramic biomaterials. Biomaterials. 2002; 23:1237–47. [PubMed: 11791928]
53. Sawyer AA, Hennessy KM, Bellis SL. Regulation of mesenchymal stem cell attachment and spreading on hydroxyapatite by RGD peptides and adsorbed serum proteins. Biomaterials. 2005; 26:1467–75. [PubMed: 15522748]
54. Zhao X, Heng BC, Xiong S, Guo J, Tan TT, Boey FY, et al. In vitro assessment of cellular responses to rod-shaped hydroxyapatite nanoparticles of varying lengths and surface areas. Nanotoxicology. 2011; 5:182–94. [PubMed: 21609137]
55. Meskinfam M, Sadjadi MA, Jazdarreh H, Zare K. Biocompatibility evaluation of nano hydroxyapatite-starch biocomposites. Journal of biomedical nanotechnology. 2011; 7:455–9. [PubMed: 21830489]
56. Kulterer B, Friedl G, Jandrositz A, Sanchez-Cabo F, Prokesch A, Paar C, et al. Gene expression profiling of human mesenchymal stem cells derived from bone marrow during expansion and osteoblast differentiation. BMC genomics. 2007; 8:70. [PubMed: 17352823]
57. Robling AG, Castillo AB, Turner CH. Biomechanical and molecular regulation of bone remodeling. Annual review of biomedical engineering. 2006; 8:455–98.
58. Lian JB, Stein GS, Javed A, van Wijnen AJ, Stein JL, Montecino M, et al. Networks and hubs for the transcriptional control of osteoblastogenesis. Reviews in endocrine & metabolic disorders. 2006; 7:1–16. [PubMed: 17051438]
59. Ghali O, Chauveau C, Hardouin P, Broux O, Devedjian JC. TNF-alpha's effects on proliferation and apoptosis in human mesenchymal stem cells depend on RUNX2 expression. Journal of bone and mineral research: the official journal of the American Society for Bone and Mineral Research. 2010; 25:1616–26. [PubMed: 20200969]
60. Pratap J, Galindo M, Zaidi SK, Vradii D, Bhat BM, Robinson JA, et al. Cell growth regulatory role of Runx2 during proliferative expansion of preosteoblasts. Cancer research. 2003; 63:5357–62. [PubMed: 14500368]
61. Galindo M, Pratap J, Young DW, Hovhannisyan H, Im HJ, Choi JY, et al. The bone-specific expression of Runx2 oscillates during the cell cycle to support a G1-related antiproliferative function in osteoblasts. The Journal of biological chemistry. 2005; 280:20274–85. [PubMed: 15781466]
62. Sibilla P, Sereni A, Aguiari G, Banzi M, Manzati E, Mischiati C, et al. Effects of a hydroxyapatite-based biomaterial on gene expression in osteoblast-like cells. Journal of dental research. 2006; 85:354–8. [PubMed: 16567558]
63. Mizuno M, Fujisawa R, Kuboki Y. Type I collagen-induced osteoblastic differentiation of bone-marrow cells mediated by collagen-alpha2beta1 integrin interaction. Journal of cellular physiology. 2000; 184:207–13. [PubMed: 10867645]
64. Lian JB, Stein GS. Concepts of osteoblast growth and differentiation: basis for modulation of bone cell development and tissue formation. Critical reviews in oral biology and medicine: an official publication of the American Association of Oral Biologists. 1992; 3:269–305. [PubMed: 1571474]
65. Phipps MC, Clem WC, Catledge SA, Xu Y, Hennessy KM, Thomas V, et al. Mesenchymal stem cell responses to bone-mimetic electrospun matrices composed of polycaprolactone, collagen I and nanoparticulate hydroxyapatite. PloS one. 2011; 6:e16813. [PubMed: 21346817]

66. Ravichandran R, Ng CC, Liao S, Pliszka D, Raghunath M, Ramakrishna S, et al. Biomimetic surface modification of titanium surfaces for early cell capture by advanced electrospinning. Biomedical materials. 2011; 7:015001. [PubMed: 22156014]

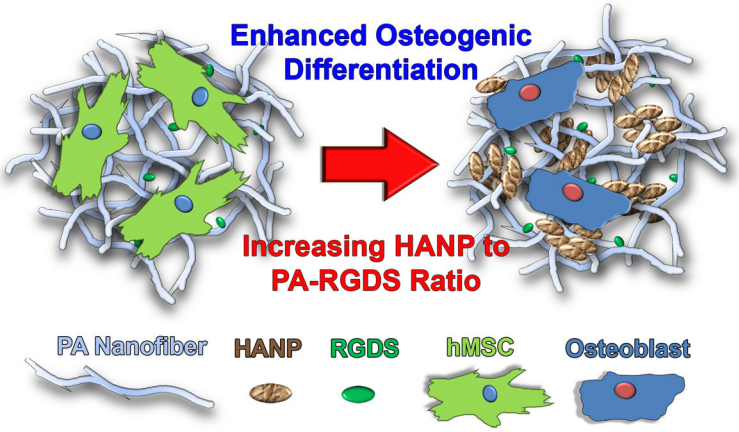

Figure 1. General Scheme

Bone analogous nanomatrix composites in which HANPs are encapsulated by PA nanofibers tailored with the RGDS binding motif to mimic the native ECM of bone were fabricated. These composites were fabricated at various HANP to PA-RGDS ratios to assess how variations in the nanomatrix composition influence the osteogenic differentiation of hMSCs. It was hypothesized that the composites with the highest HANP to PA-RGDS ratio are the most conducive to osteogenic differentiation.

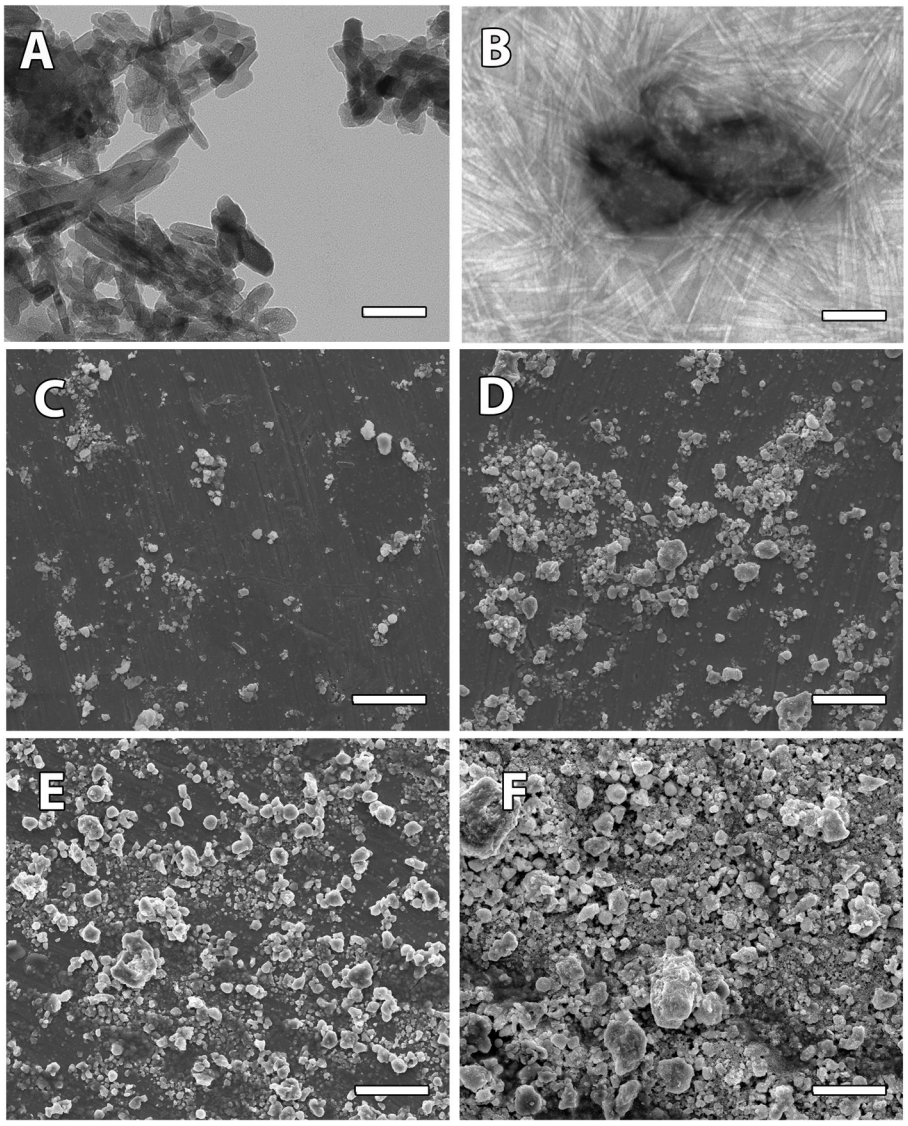

Figure 2. Characterization of nanomatrix composites

TEM images of (A) HANPs and (B) PA-RGDS (16% HANP) at 42000×. SEM Images of (C) PA-RGDS (16% HANP) (D) PA-RGDS (33% HANP) (E) PA-RGDS (50% HANP) and (F) PA-RGDS (66% HANP) at 1000×. Scale bars represent 100 nm for TEM and 50μm for SEM respectively. Considered together, TEM and SEM images demonstrate aggregates of varying size and distribution made up of HANPs enmeshed within PA nanofibers.

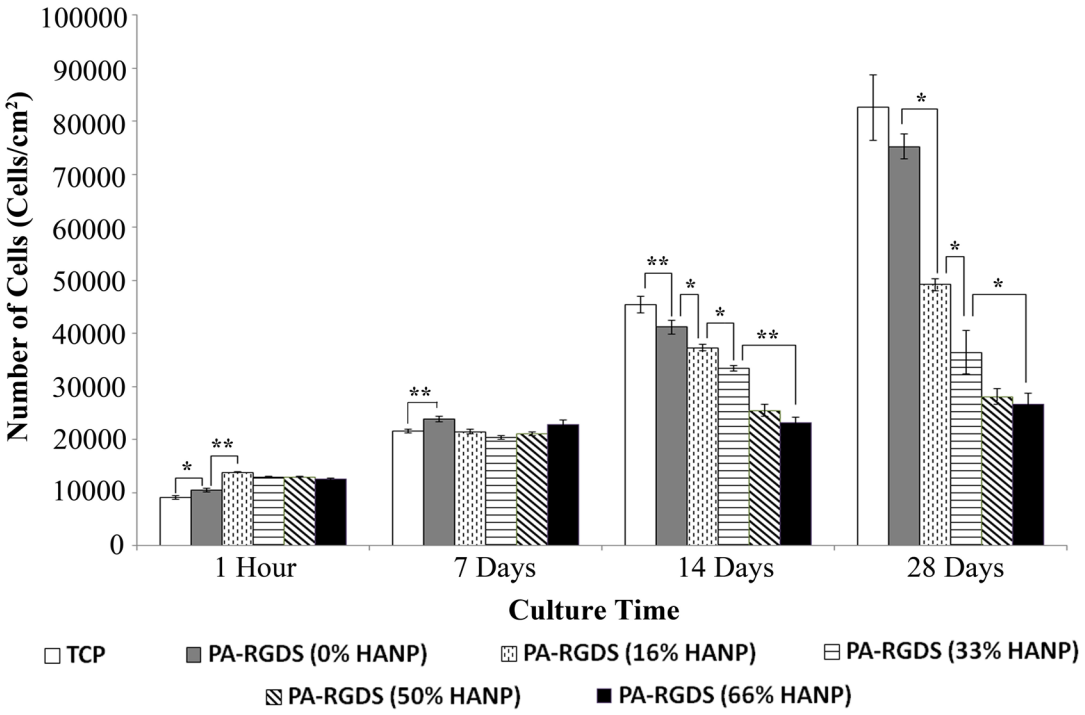

Figure 3. Initial Attachment and Cellularity over 28 days

Cells were first assessed for attachment on all surfaces at 1 hour, following which, they were assessed for cellularity over 28 days. Overall, nanomatrix composite conditions exhibited greater attachment than PA-RGDS alone. Over the 28 day time frame, there were step-wise decreases in cellularity, with differences first manifesting at the 14 day time point. Values are expressed as a mean ± standard error of measurement (* $p < 0.05$, **$p<0.01$).

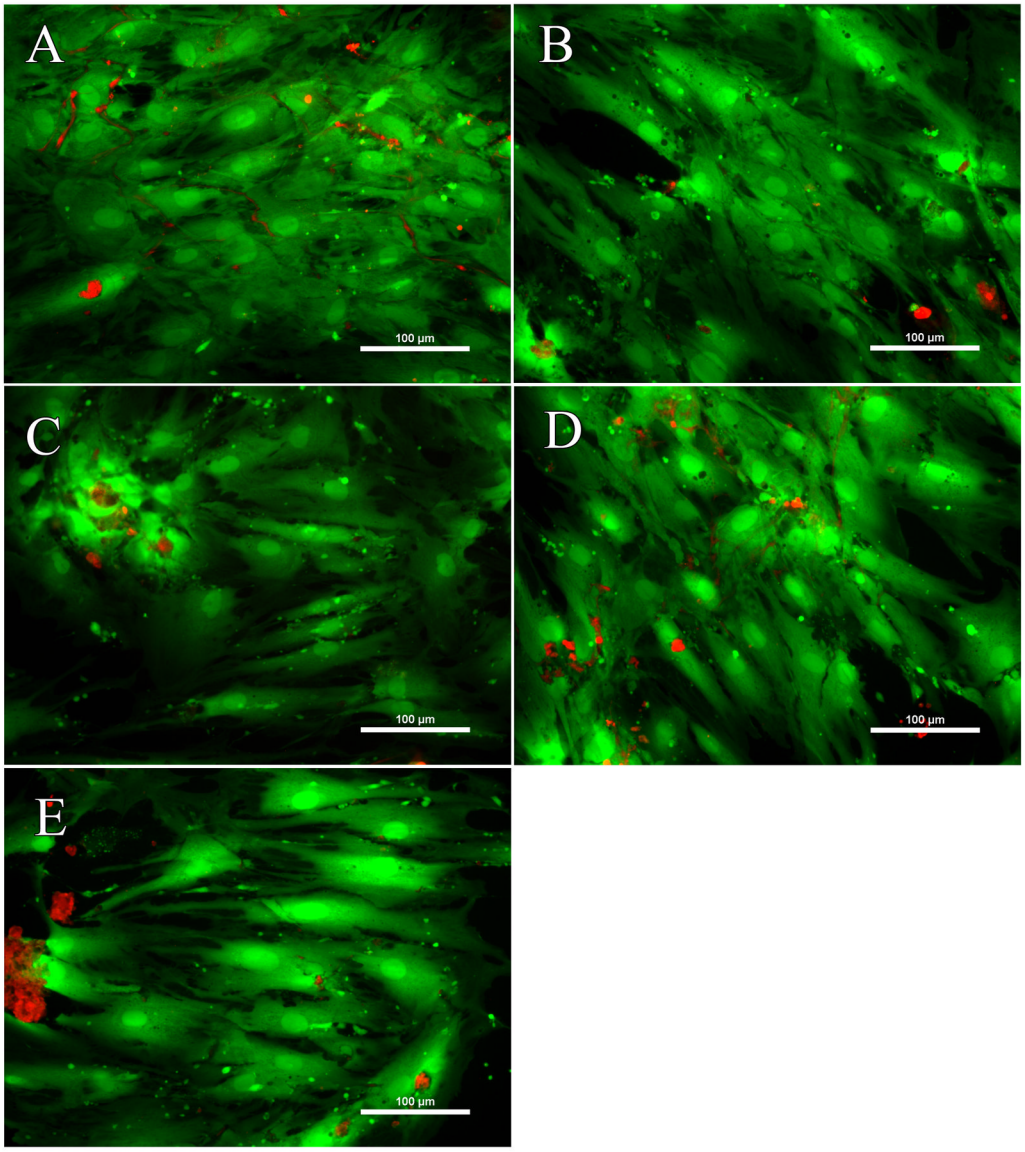

Figure 4. Cellular viability over 7 days

(A) PA-RGDS, (B) PA-RGDS (16% HANP), (C) PA-RGDS (33% HANP), (D) PA-RGDS (50% HANP), and (E) PA-RGDS (66% HANP). Cells on all culture conditions were imaged utilizing a Live/Dead assay kit over 7 days. Overall, there were no differences in terms of viability between the nanomatrix composites and PA-RGDS. Images are taken at 20×. Scale bars represent 100 μM.

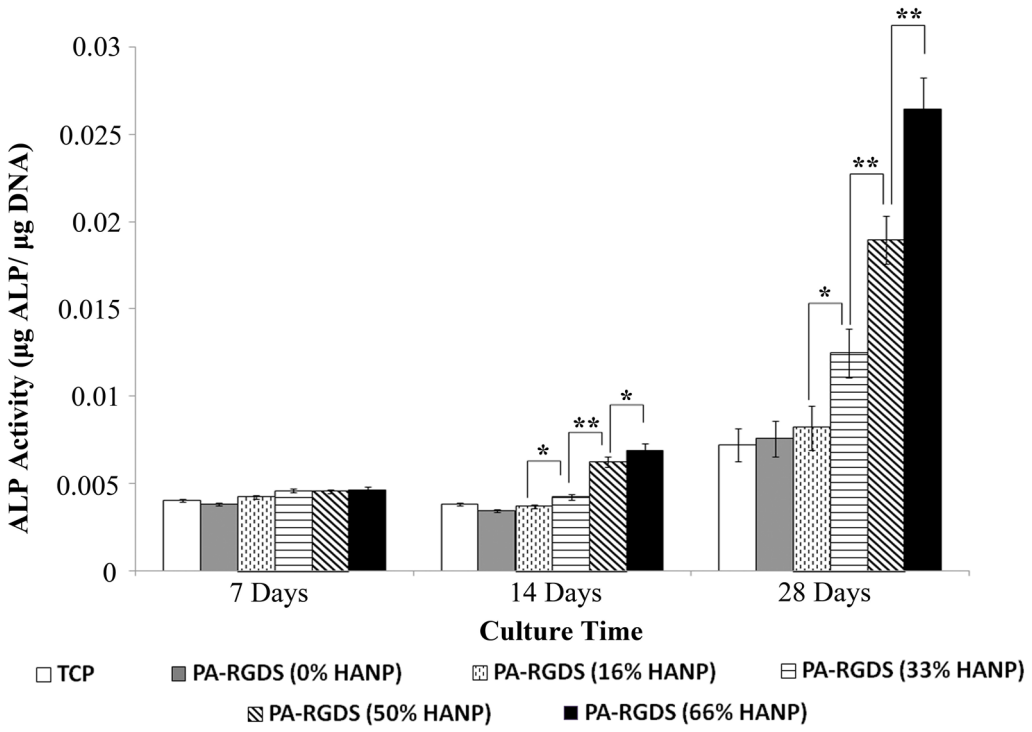

Figure 5. ALP Activity over 28 days

Over the 28 day time frame, there were step-wise increases in ALP activity based on increases in the HANP to PA-RGDS ratios. The 66% HANP nanomatrix composite condition demonstrated the greatest ALP activity over the course of the experiment. Values are expressed as a mean ± standard error of measurement (*p<0.05, **p<0.01).

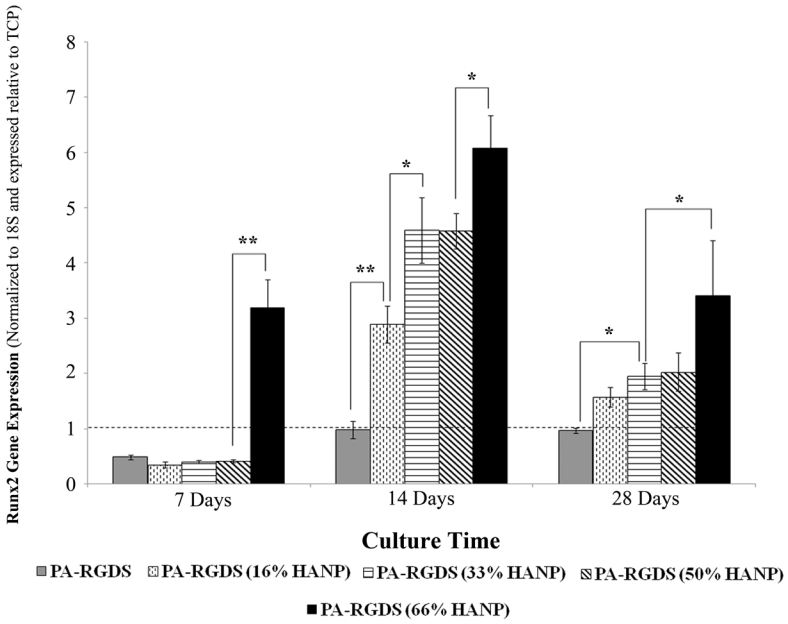

Figure 6. Gene expression profile for Runx2 over 28 days

Runx2 gene expression peaked at the day 14 time point on all conditions, with enhancements linearly increasing based on increasing HANP to PA-RGDS ratios. The early expression for the 66% HANP condition at day 7 demonstrates its improved capability for osteoinduction relative to other conditions. Values are expressed as a mean ± standard error of measurement relative to TCP (dashed line) for all incubation periods. ($p < 0.05$, $^{**}p<0.01$).

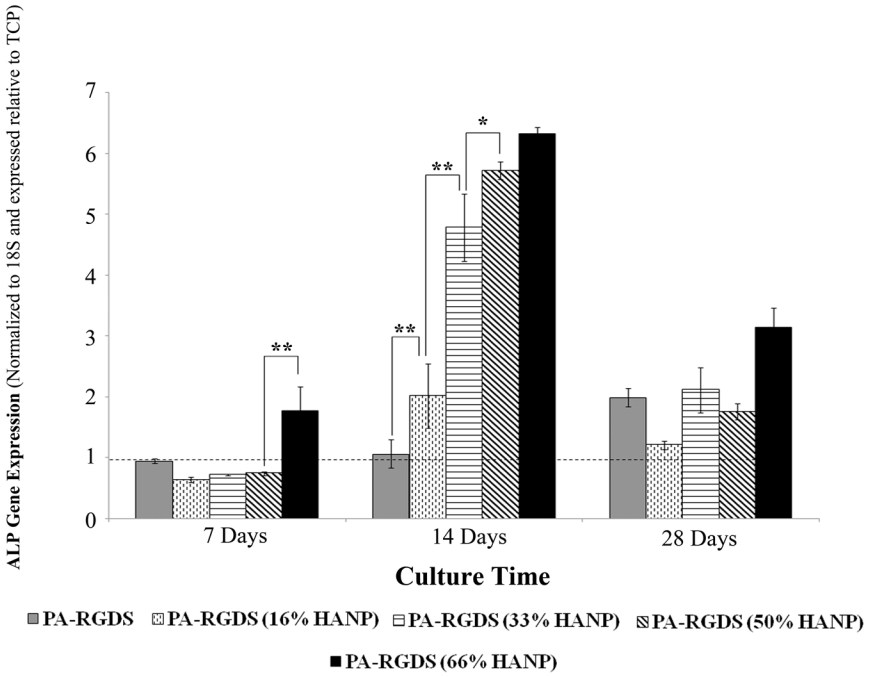

Figure 7. Gene expression profile for ALP over 28 days

At day 7, the 66% HANP containing composite had the greatest expression. For all conditions, ALP peaked at day 14 with greater expression exhibited in conditions with higher HANP to PA-RGDS ratios. Values are expressed as a mean ± standard error of measurement relative to TCP (dashed line) for all incubation periods. (*$p < 0.05$, **$p<0.01$).

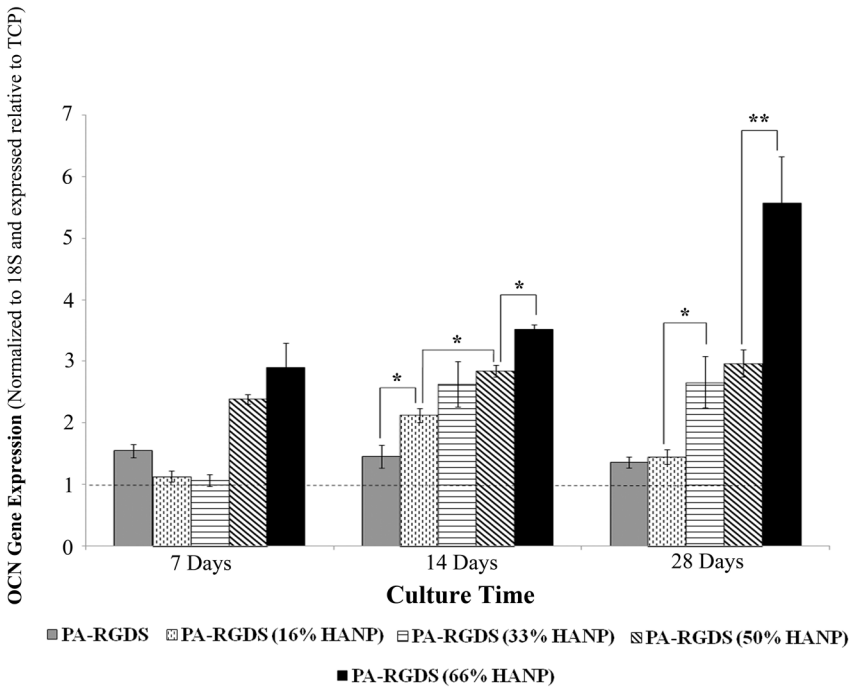

Figure 8. Gene expression profile for OCN over 28 days

For all conditions, OCN expression is the most pronounced at the 14 and 28 day time points with expression increasing in a step-wise fashion based on increasing HANP to PA-RGDS ratios. OCN expression is greatest at day 28, with the 66% HANP containing composite demonstrating the greatest increase. Values are expressed as a mean ± standard error of measurement relative to TCP (dashed line) for all incubation periods. (*$p < 0.05$, **$p<0.01$).

Table 1

Experimental Conditions

Control	**PA Concentration (mg/mL)**
$CH_3(CH_2)_{14}CONH$–GTAGLIGQ–RGDS (PA-RGDS)	1
Variable	**HANP Concentration (mg/mL)**
PA-RGDS (16% HANP)	0.19
PA-RGDS (33% HANP)	0.49
PA-RGDS (50% HANP)	1
PA-RGDS (66% HANP)	1.94

Table 2

Primers for RT-PCR

Primer	Abbreviation	Sequence (5′–3′)	GenBank identification
Runt related transcriptional factor 2	Runx2		NM_004348
Sense		AGA TGA TGA CAC TGC CAC CTC TG	
Antisense		GGG ATG AAA TGC TTG GGA ACT	
Alkaline Phosphatase	ALP		NM_000478
Sense		ACC ATT CCC ACG TCT TCA CAT TT	
Antisense		AGA CAT TCT CTC GTT CAC CGC C	
Osteocalcin	OCN		NM_199173
Sense		CAA AGG TGC AGC CTT TGT GTC	
Antisense		TCA CAG TCC GGA TTG AGC TCA	
18S rRNA	18S		X_03205.1
Sense		CGG CTA CCA CAT CCA AGGAA	
Antisense		GCT GGA ATT ACC GCG GCT	